Journal of proteome research

pubs.acs.org/jpr

Article

Proteomic Characterization of Transfusable Blood Components: Fresh Frozen Plasma, Cryoprecipitate, and Derived Extracellular Vesicles via Data-Independent Mass Spectrometry

Ji Hui Hwang,* Andrew Lai, John-Paul Tung, Damien G Harkin, Robert L Flower, and Natalie M Pecheniuk

Cite This: *J. Proteome Res.* 2024, 23, 4508−4522

Read Online

ACCESS | Metrics & More | Article Recommendations | Supporting Information

ABSTRACT: Extracellular vesicles (EVs) are a heterogeneous collection of particles that play a crucial role in cell-to-cell communication, primarily due to their ability to transport molecules, such as proteins. Thus, profiling EV-associated proteins offers insight into their biological effects. EVs can be isolated from various biological fluids, including donor blood components such as cryoprecipitate and fresh frozen plasma (FFP). In this study, we conducted a proteomic analysis of five single donor units of cryoprecipitate, FFP, and EVs derived from these blood components using a quantitative mass spectrometry approach. EVs were successfully isolated from both cryoprecipitate and FFP based on community guidelines. We identified and quantified approximately 360 proteins across all sample groups. Principal component analysis and heatmaps revealed that both cryoprecipitate and FFP are similar. Similarly, EVs derived from cryoprecipitate and FFP are comparable. However, they differ between the originating fluids and their derived EVs. Using the R-package MS-DAP, differentially expressed proteins (DEPs) were identified. The DEPs for all comparisons, when submitted for gene enrichment analysis, are involved in the complement and coagulation pathways. The protein profile generated from this study will have important clinical implications in increasing our knowledge of the proteins that are associated with EVs derived from blood components.

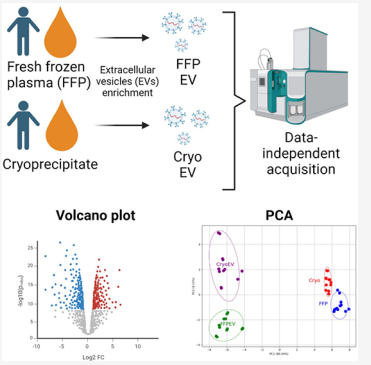

KEYWORDS: *fresh frozen plasma, cryoprecipitate, extracellular vesicles, mass spectrometry, data independent acquisition*

Downloaded via UNIV OF QUEENSLAND on September 1, 2025 at 02:54:25 (UTC).
See https://pubs.acs.org/sharingguidelines for options on how to legitimately share published articles.

INTRODUCTION

Extracellular vesicles (EVs) are a heterogeneous group of nanosized, lipid bilayer-enclosed particles (50−1000 nm) that are released by nearly every cell type. They are present in various body fluids, including blood, urine, saliva, and cerebrospinal fluid.[1−3] EVs transport a diverse range of molecular cargo, including proteins, lipids, and nucleic acids, and are critical mediators of intracellular communication in both normal physiology and pathophysiology.[4,5] As such, they can provide invaluable insights into cellular processes, signaling pathways, and potential disease biomarkers such as cancers, pregnancy complications, and cardiovascular diseases.[6−8]

Over the last two decades, there has been a dramatic surge in publications related to EVs. This trend is particularly evident in studies using mass spectrometry (MS)-based protein analysis.[9,10] High-throughput proteomics is employed to investigate the complex protein content of EVs derived from various body fluids and cell types. In addition, this protein cargo represents a promising source of biomarkers for disease diagnosis and monitoring.[11] While plasma is the most extensively studied fluid for EV disease biomarkers, the limited quantity of EVs in plasma complicates their investigation.[12] Consequently, prior to molecular analysis, it is crucial to isolate EVs for optimal yields and purity. This is because the abundant proteins in plasma can interfere with the proteomic characterization of EVs.[12−14]

Plasma, a major component of blood, is an abundant source of EVs. However, the association of EVs with specific blood components intended for transfusion, such as fresh frozen plasma (FFP) and cryoprecipitate, remains under explored. Previous studies have focused on other blood components, such as red blood cells and platelets.[15,16] These transfusion blood components, in a clinical setting, have unique processing and storage protocols that might influence their EV content and characteristics. Given the complexities in studying the EV content and characteristics in different blood components like FFP and cryoprecipitate, advanced analytical methodologies have become crucial. The sequential window acquisition of all theoretical fragment ion spectra (SWATH), an approach in mass spectrometry (MS), steps into this arena as a promising

Received: May 21, 2024
Revised: August 15, 2024
Accepted: August 29, 2024
Published: September 10, 2024

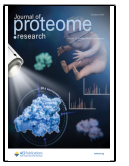

ACS Publications

© 2024 American Chemical Society

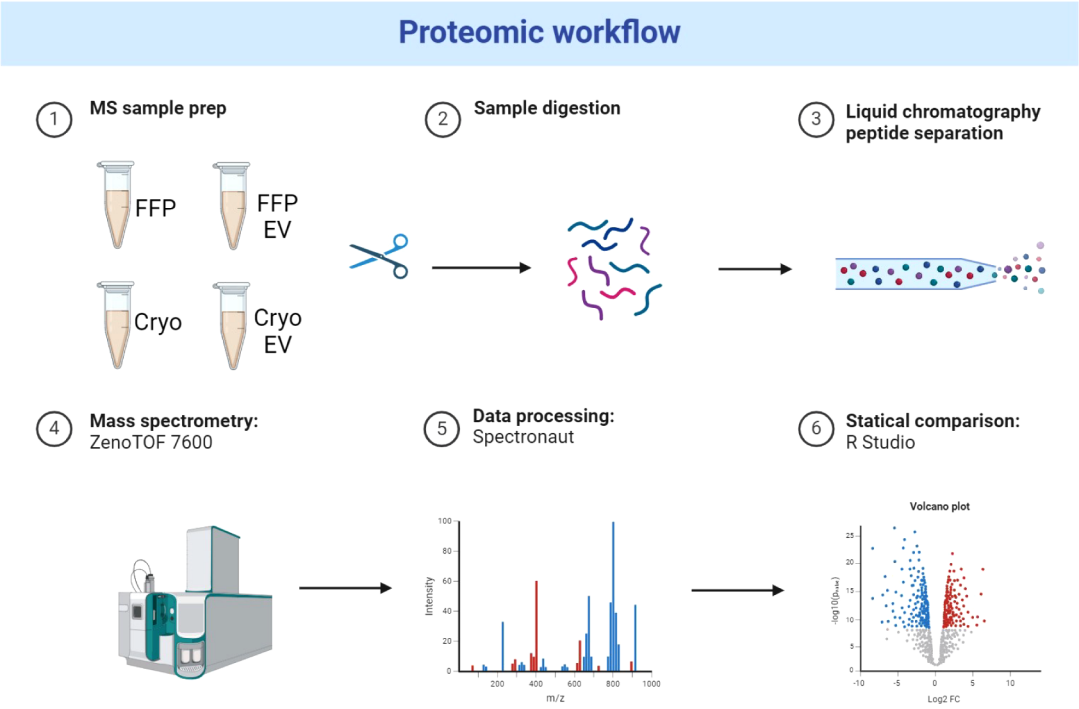

Figure 1. Schematic overview of mass spectrometry workflow. EVs were isolated from FFP and cryoprecipitate and underwent MS sample preparation, which involved in-solution protein digestion. The digested peptides were then processed for acquisition on an LC-MS/MS system. The raw data were processed using Spectronaut, and this process was subsequently searched, visualized, and analyzed using R Studio.

tool for the in-depth proteomic analysis of these biological samples.

SWATH also known as data-independent acquisition (DIA) in MS, has emerged as an unbiased and alternative technology for the proteomic analysis of biological samples. It addresses certain limitations inherent to conventional data-dependent acquisition (DDA)-based analysis.[17,18] DIA creates a comprehensive fragmentation map of all detectable precursors, enabling the accurate quantification of a given sample. It achieves this by dividing peptide precursor ions into multiple consecutive mass windows for fragmentation.[19] Furthermore, DIA offers advantages including the requirement for lesser quantities of clinical samples, provision of sufficient proteome coverage with quantitative consistency, and analytic accuracy.[17,20,21] However, the raw data generated from DIA is more complex compared to traditional DDA and therefore requires increased computational power and more elaborate software and statistical tools.

In our study, we performed a proteomics analysis of cryoprecipitate, FFP and EVs derived from those blood components using DIA. The purpose of our study was to generate a proteomic map of these samples using a DIA approach and to identify differentially expressed proteins. This investigation aimed to gain insights into EVs within FFP and cryoprecipitate but also highlights areas of limited understanding of their potential significance in transfusion medicine.

EXPERIMENTAL PROCEDURES

Experimental Design and Rationale

A total of 48 samples were examined in this study, including 5 individual units of FFP, a pooled FFP sample comprising these 5 units, 6 EV samples derived from the individual and pooled FFP, 5 individual units of cryoprecipitate, a pooled cryoprecipitate (from those 5 units), and 6 EV samples from these cryoprecipitates.

All mass spectrometry data were acquired in a single uninterrupted sequence. Proteomic data were generated using data-independent acquisition (DIA). The workflow used for this study is illustrated in Figure 1. Additional information regarding the samples analyzed, data acquisition, and processing procedures is provided below.

Ethics, Sample Collection, Preparation, and EV Isolation and Characterization

This study was approved by the Australian Red Cross Lifeblood Ethics Committee (approved project 2020#08) and the University Human Research Ethics Committee (UHREC) at Queensland University of Technology (approved project 2000000548). Australian Red Cross Lifeblood supplied five units of cryoprecipitate derived from the O-positive whole blood and five units each of FFP from the O-positive and O-negative whole blood, all sourced from different single donors.

EV ISOLATION AND CHARACTERIZATION

EV Isolation from FFP and Cryoprecipitate

To isolate EVs from FFP or cryoprecipitate, 0.5 mL of each unit was centrifuged at 2000 × *g* for 20 min at 4 °C to pellet any large debris large aggregates. The supernatant was further centrifuged at 10 000 × *g* for 40 min at 4 °C to deplete larger EVs. This supernatant was subsequently subjected to size-exclusion chromatography (SEC) using qEVoriginal 70 nm columns (Izon, Christchurch, New Zealand) in conjunction with the automated fraction collector (AFC) as per the manufacturer's instructions. The collected EV fractions totaling 1.5 mL were then concentrated down to 0.1 mL using ultrafiltration with an Amicon Ultra-15 filter with a 100 kDa molecular weight cutoff (Cat. No. UFC910008; Merck, Burlington, MA, USA). EVs were then verified based upon criteria established by the International Society of Extracellular Vesicles using nanoparticle

https://doi.org/10.1021/acs.jproteome.4c00417
J. Proteome Res. 2024, 23, 4508−4522

tracking analysis (to obtain particle size and concentrations), Western blotting (for evidence of EV-enriched protein markers) and cryogenic transmission electron microscopy (to assess morphology).[22]

Nanoparticle Tracking Analysis

The size distribution and concentration of particles in blood components and EV-purified fractions were measured using a Nanosight NS300 instrument (Malvern Technologies, Malvern, UK). Samples were diluted 1:100 in 0.1 μm-filtered PBS. Three 60 s videos were recorded using camera level of 13 and a detection threshold of four. Each replicate was measured at a constant flow rate of 50 units/min. The recorded videos were processed using NTA software, version 3.4.4.

Protein Quantification

A bicinchoninic acid (BCA) protein assay (Thermo Fisher Scientific, Rockford, IL, USA) was performed to determine the protein concentration within each sample, according to the manufacturer's instructions using bovine serum albumin as a standard.

Cryogenic Transmission Electron Microscopy (Cryo-TEM)

EV samples were imaged by cryo-TEM. Specimens were prepared using the Leica EM GP2 robotic vitrification system under controlled temperature (22 °C) and relative humidity (95%). A 3 μL dispersion of EVs was applied onto a carbon coated perforated Formvar film supported on a 200 mesh copper TEM grid. Any excess solution was automatically blotted for a period of 3−3.5 s and swiftly plunged into liquid ethane near its freezing point (−183 °C). The grids were stored under liquid nitrogen until imaging. The samples were imaged using a Jeol Cryo ARM 200 (JEM-Z200FSC) transmission electron microscope (TEM) in a frozen hydrated state at −176 °C. The microscope was equipped with a cold field emission gun (FEG) and an in-column Omega energy filter. The images were captured with zero energy loss at an acceleration voltage of 200 kV and a filter setting of 20 eV. To ensure minimal exposure, the images were recorded under low-dose conditions using the SerialEM software[23] and a Gatan K2 direct detector camera.

Western Blot

An equivalent of 8 μg of EVs derived from FFP and cryoprecipitate were mixed with NuPAGE LDS sample buffer and reducing agent and then heated at 70 °C for 10 min. The samples were then loaded into each well of precast NuPAGE Bolt 4−12% polyacrylamide gels (Thermo Fisher Scientific, Rockford, IL, USA) and run with NuPAGE MES-PAGE running buffer. A control sample containing enriched membrane-associated proteins isolated was included (Mem-PER Plus Membrane Protein Extraction Kit, ThermoFisher, Rockford, IL, USA). After electrophoresis, the separated proteins were transferred onto PVDF membranes at 100 V for 60 min. The membranes were then blocked using Odyssey blocking buffer (OBB, Li-COR, USA) for 1 h at room temperature. Primary antibodies were diluted 1:1000 with the OBB and incubated overnight at 4 °C. The following primary antibodies were utilized: anti-CD9 (no. 263019, Abcam, Waltham, MA, USA), anti-CD81 (no. 109201, Abcam, Waltham, MA, USA), antiflotillin 1 (no. 3253, Cell Signaling, Danvers, MA, USA), and antifibronectin (no. 2413, Abcam, Waltham, MA, USA), and the blot was washed with TBST for 5 min; this process was repeated twice. Secondary antibodies (Goat antirabbit #925-32211, Li-COR) were diluted 1:15 000 in OBB and incubated for 1 h at room temperature in the dark. The blot was then washed with TBST six times, each for 5 min. Images were captured on an LI-COR Odyssey instrument using Image Studio software, version 5.2 (LI-COR).

Tryptic Digestion of Samples

Approximately 10 μg of each sample, as quantified by the bicinchoninic acid (BCA) assay, was used for in-solution digestion using the EasyPep MS Sample Prep Kit (Cat. No. A45733, Thermo Fisher Scientific, MA, USA). This kit contains a complete set of proprietary reagents needed for the tryptic digestion of samples. The samples were lysed, reduced, and alkylated in Eppendorf low protein binding tubes following the manufacturer's instructions. This was followed by digestion with a Lys-C/trypsin mix at a 1:20 Lys-C/Lys-C/trypsin to sample ratio for 3 h. The resulting tryptic peptides were subjected to detergent removal and desalted using the supplied detergent removal solid phase extraction columns. The digested samples were dried and stored at −80 °C until mass spectrometry analysis.

Global Proteomics by LC-MS/MS

Peptide extracts were resuspended in 0.1% v/v formic acid (FA) in water and analyzed using an Eksigent 400 liquid-chromatography (LC) system coupled with a 7600 ZenoTOF mass spectrometer (SCIEX). The mobile phase solvents were 0.1% FA in water (A) and 0.1% FA in ACN (B). The microflow LC was configured in a "trap-elute" mode, where the peptides were first concentrated on a trapping column (Micro Trap C18 10 × 0.3 mm, Cat. No. 05N-4252-AC, Phenomenex, USA) for 10 min in 100% solvent A at a flow rate of 10 μL/min. Subsequently, being eluted into the analytical column (BIOshell 15 cm × 300 μm, 2.7 μm 160 Å Peptide C18, Cat. No. 67093-U, Merck) for separation and subsequent MS detection. A 15.5 min linear gradient (5−35% B) was used for elution at a flow rate of 5 μL/min, with the oven temperature set at 40 °C and the autosampler temperature at 10 °C. Full details can be found in Supplementary Table S1.

The 7600 ZenoTOF was equipped with an OptiFlow Turbo V ion source and operated in SWATH mode with the Zeno trap activated. The ion source conditions were as follows: ionization voltage 5500 V, positive polarity, temperature 150 °C, ion source gas 1 at 20 psi, ion source gas 2 at 15 psi, and curtain gas at 35 psi. A SWATH acquisition scheme with 65 variable windows covering 400−750 m/z was used with an MS2 accumulation time of 10 ms (Supplementary Table S2).

Each sample was injected in duplicate. Samples were injected no more than 2 days after being loaded into the autosampler. The performance of the mass spectrometer was monitored before each sample was introduced using injections of HeLa protein digest (Cat. No. 88329, Thermo Fisher Scientific) and K562 protein digest (Cat. No. 6951, Promega, WI, USA). External calibration was performed every three to eight runs using the automatic calibration function and ESI positive calibration solution for the SCIEX X500B system (Cat. No. 5049910, SCIEX).

Data Processing

All mass spectrometry DIA raw data were processed with the commercial package Spectronaut (18.3.230830.50606)[24] using the default factory settings provided in the user interface (as detailed in Supplementary Figure S1). The Direct DIA+ library-free workflow was used, using the *Homo sapiens* reference proteome FASTA file from Uniprot (UP000005640, downloaded 08 2023). A custom reporting schema was used to export

https://doi.org/10.1021/acs.jproteome.4c00417
J. Proteome Res. 2024, 23, 4508−4522

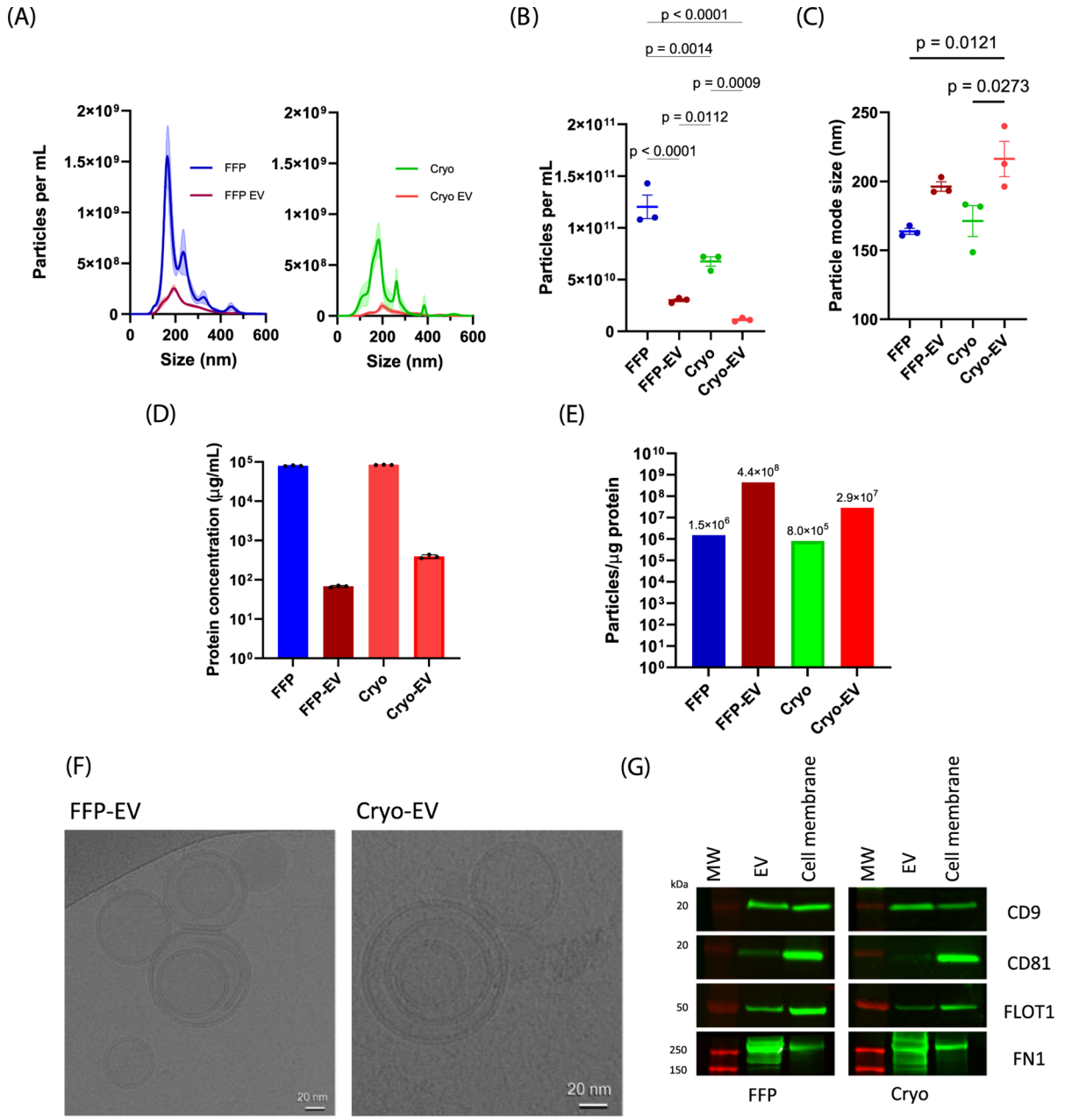

Figure 2. Characterization of FFP, cryoprecipitate, and extracellular vesicles by four different methods. (A) Representative plots displaying the concentration and size distribution of FFP, FFPEV, cryoprecipitate, and cryoprecipitate-EV, as determined through nanoparticle tracking analysis. (B,C) Graph representing the average mode of particle diameter (B) and concentration (in particles/mL) for each sample (n = 3 samples per group; C). (D) Representative plots illustrating the protein concentration of four distinct samples. (E) Assessment of EV sample purity by calculating the ratio of EV particle count to protein concentration. (F) Cryogenic transmission electron microscopy of purified EVs from FFP and cryoprecipitate. Scale bar represents 20 nm. (G) Western blot analysis indicating the presence of CD9, CD81, FLOT1, and FN1 in purified EVs and cell membrane control. The full uncropped images can be found in Supplementary Figure S4. Results were statistically compared by ordinary one-way ANOVA, followed by Tukey's multiple comparisons test. A p value of <0.05 was considered statistically significant. FFP: fresh frozen plasma; Cryo: cryoprecipitate; FFPEV: extracellular vesicles derived from fresh frozen plasma; Cryo-EV: extracellular vesicles derived from cryoprecipitate; MW: molecular weight.

the processed data from Spectronaut for downstream analysis (Supplementary Figure S2). The mass spectrometry proteomics data have been deposited to the ProteomeXchange Consortium via the PRIDE (11) partner repository with the data set identifier PXD052003.

Data Analysis and Visualization

Unless otherwise specified, analyses were performed in R (v4.3.0)[25] and RStudio (v2023.03.1 build 446).[26] The Mass Spectrometry Downstream Analysis Pipeline (MS-DAP, version 1.0.6), an R package, was used to process data from Spectronaut, which included raw peak area information for normalization and differential expression analysis (DEA).[27] The full analysis settings used were the quick start as recommended by the developer of the package (Supplementary Figure S3). A key feature of MS-DAP is its capability to employ multiple statistical models for DEA. In this study, we used DEqMS,[28] MS-EmpiRe,[29] and MSqRob[30] for this purpose. A protein was considered differentially expressed if identified by at least two of these three models. Selected figures were generated using

https://doi.org/10.1021/acs.jproteome.4c00417
J. Proteome Res. 2024, 23, 4508−4522

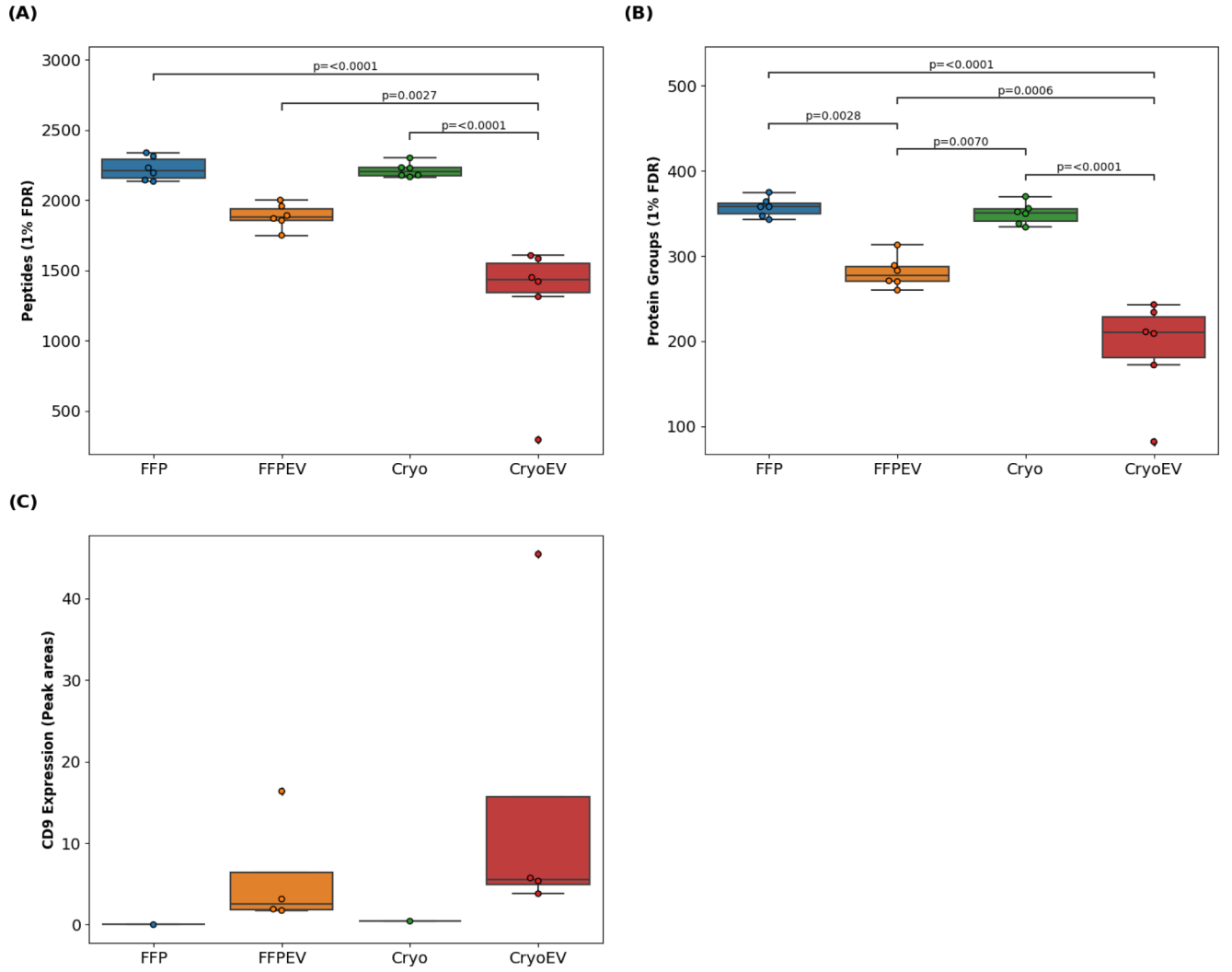

Figure 3. Peptides and proteins detected in FFP, cryoprecipitate, and derived EVs. (A) The number of detected peptides and (B) proteins at 1% FDR. (C) The normalized CD9 peak areas were extracted to demonstrate the enrichment of CD9, an EV-associated marker, in these samples. Cryo: cryoprecipitate; FFP: fresh frozen plasma; CryoEV: EVs derived from cryoprecipitate; FFPEV: EVs derived from FFP; FDR: false discovery rate.

PyCharm (v2023.3),[31] an integrated environment used for programming in Python using the plotting library Matplotlib (v3.8.2)[32] and Seaborn (v0.11.2).[33] One-way ANOVA followed by Dunnett's multiple comparisons test was performed using GraphPad Prism version 10.0.2 (GraphPad Software, Boston, MA, USA). The list of the top 100 proteins previously associated with EVs was obtained from Vesiclepedia.[34] Proteins associated with coagulation cascades (entry: hsa04610) were downloaded from the Kyoto Encyclopedia of Genes and Genomes (KEGG) database.[35] Gene ontology and pathway enrichment analysis was conducted using clusterProfiler[36] and pathview[37] via the online portal SRplot.[38]

RESULTS

Characterization of Extracellular Vesicles from FFP and Cryoprecipitate

Nanoparticle tracking analysis (Figure 2A,B) demonstrated that particle concentrations were higher in FFP compared to cryoprecipitate (1.20×10^{11} vs 6.75×10^{10} particles/mL; $p = 0.0014$). The isolated EV samples had a lower particle concentration compared to those of the original blood components from which they were derived. For FFP, there was a reduction from 1.20×10^{11} to 3.0×10^{10} particles/mL ($p < 0.0001$). In the case of cryoprecipitate, the reduction was from 6.75×10^{10} to 1.12×10^{10} particles/mL ($p = 0.0009$). However, the concentrations of particles in FFPEV and cryoprecipitate-EV were not significantly different.

The average mode sizes for the particles within FFP and cryoprecipitate were similar: 163 and 171 nm, respectively ($p > 0.05$; Figure 2C). The isolated EV samples had a larger average particle mode size compared to the blood components from which they were isolated from. The FFPEV had an average particle mode size of 196 nm, while cryoprecipitate-EV had an average size of 216 nm. When comparing particle mode sizes between the neat sample and their derived EVs, there was a significant difference between cryoprecipitate and cryoprecipitate-EV ($p = 0.0273$). Although the FFPEV was slightly larger in particle mode than the FFP, this difference was not statistically significant.

Protein concentrations in the four different samples were measured. FFP and cryoprecipitate contained 79 672.7 and 84 292.5 μg/mL, respectively. Moreover, the protein concentrations of FFPEV and cryoprecipitate-EV were 67.6 μg/mL and 390.6 μg/mL, respectively (Figure 2D). Based on the particle and protein concentration, we assessed the purity of each

https://doi.org/10.1021/acs.jproteome.4c00417
J. Proteome Res. 2024, 23, 4508−4522

sample. Both FFP (1.5×10^5 particles/μg protein) and cryoprecipitate (8.0×10^5 particles/μg protein) indicated lower purity, while there was an enrichment of particles in FFPEV and cryoprecipitate-EV to 4.4×10^8 particles/μg and 2.9×10^7 particles/μg, respectively. This clearly demonstrated the enrichment of EVs compared to that of the originating blood component. Notably, FFPEV revealed greater purity than cryoprecipitate-EV, as its particle concentrations were three times higher, and its protein concentration was 5.8 times greater than that of cryoprecipitate-EV (Figure 2E). Morphological assessment of FFPEV and cryoprecipitate-EV using cryogenic transmission electron microscopy (cryo-TEM) allowed the preservation of samples in their native hydrated states. This method revealed circular particles containing a membrane bilayer, indicative of EVs. Additionally, it showed an average size of particles ranging approximately from 50 to 100 nm (Figure 2F). Finally, based on MISEV 2023 guidelines,[22] Western blot analysis was performed on the isolated EV samples to confirm the presence of EV-associated proteins: (1) transmembrane proteins CD9 and CD81, (2) FLOT1, which is a cytosolic protein with membrane-association capacity, and (3) FN1 was used to assess major components of coisolated non-EV protein (Figure 2G). The uncropped Western blot images can be found in Supplementary Figure S4. Taken all together, these results allowed us to classify the isolated particles as EVs and confirmed the successful enrichment of EVs from both FFP and cryoprecipitate.

Peptide and Protein Identification and Quantification

The proteomic profiles of FFP, FFPEV, Cryo, and CryoEV were analyzed for comprehensive proteome characterization via DIA mass spectrometry. A total of 3081 peptides mapping to around 360 proteins were identified with a 1% false discovery rate (FDR) across all the samples (Supplementary Figure S5). When assessing each sample type individually (Figure 3), the number of peptides identified in FFP was the highest, with a mean of 2224.3, followed closely by those in cryoprecipitate at 2212.8 (Figure 3A). For the EVs, 1886.5 peptides were identified in EVs derived from FFP, while EVs derived from cryoprecipitate possessed at least at 1277.2. Notably, no significant differences were observed in the number of peptides associated with FFP and those derived from its EVs. However, EVs derived from cryoprecipitate had significantly fewer peptides compared to cryoprecipitate ($p < 0.0001$). Furthermore, a significant difference was observed in the peptide numbers between EVs derived from FFP and cryoprecipitate ($p = 0.0027$).

In terms of the proteins, we identified 357.5 and 350 in FFP and cryoprecipitate, respectively (Figure 3B). A notable reduction in protein numbers was found in EVs from FFP compared to FFP, at 281 ($p = 0.0028$). EVs from cryoprecipitate followed the same trend, with proteins identified at 191.8, a significant reduction compared to cryoprecipitate ($p < 0.0001$). Moreover, a significant difference in protein numbers was observed between EVs from FFP and cryoprecipitate ($p = 0.0006$).

We also investigated CD9, a common EV protein marker across the four sample groups. As anticipated, CD9 protein levels were elevated in EVs from both FFP and cryoprecipitate, with levels of 7.7 and 20.1, respectively (Figure 3C). Notably, the level of CD9 expression in EVs from cryoprecipitate was approximately three times higher than that in those from FFP. In contrast, there was no detectable CD9 expression in FFP, and cryoprecipitate showed a negligible amount.

Global Proteomic Profile Reveals Differences between Samples

Proteins were ranked on the basis of their observed abundance across all the samples (Figure 4A, Supplementary Table S3).

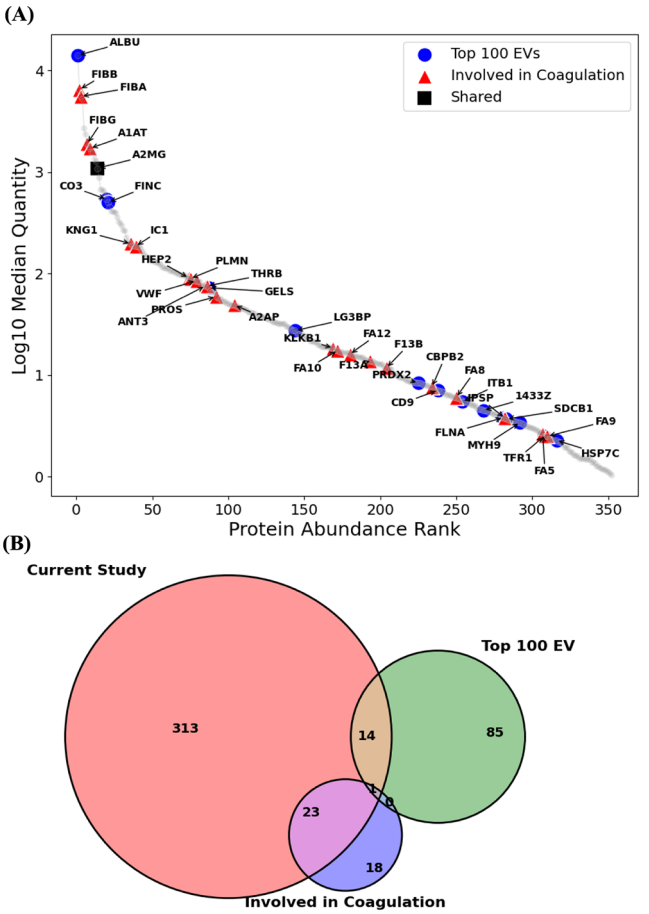

Figure 4. Protein abundance rank and Venn diagram for FFP, cryoprecipitate, and derived EVs. (A) Protein abundance ranked from high to low for all samples based on their log10 median protein group quality. Proteins (gray circles) were highlighted based on their previous association with EVs (blue circles), coagulation (red triangles), or both (black squares). (B) Venn diagram representing the number of proteins identified in this study, the top 100 EV proteins from Vesiclepedia, and proteins associated with coagulation based on KEGG pathways.

Each identified protein is a gray colored circle, with protein abundance spanning from approximately 4 logs of concentration. We have highlighted two groups of proteins that may be of interest: those involved in the coagulation pathways as denoted in the KEGG database (red triangles, Supplementary Table S4), and the top 100 proteins that have previously been identified as associated with EVs (blue circles, Supplementary Table S5). Among these, proteins from most to least abundant, including fibrinogen A alpha (FIBA), fibrinogen beta chain (FIBB), fibrinogen gamma chain (FIBG), von Willebrand factor (VWF), thyroid hormone receptor beta (THRB), factor X (FA10), factor VIII (FA8), factor V (FA5), and factor FIX (FA9), were predominantly associated with coagulation proteins. From the top 100 EV-related proteins such as albumin (ALBU), CD9 antigen (CD9), myosin heavy chain 9 (MYH9), and heat shock protein 70 family (HSP7C) as shown in Figure 4A. The Venn diagram showed that 15 proteins from the top 100 EVs and 24 proteins from the coagulation pathway were

https://doi.org/10.1021/acs.jproteome.4c00417
J. Proteome Res. 2024, 23, 4508−4522

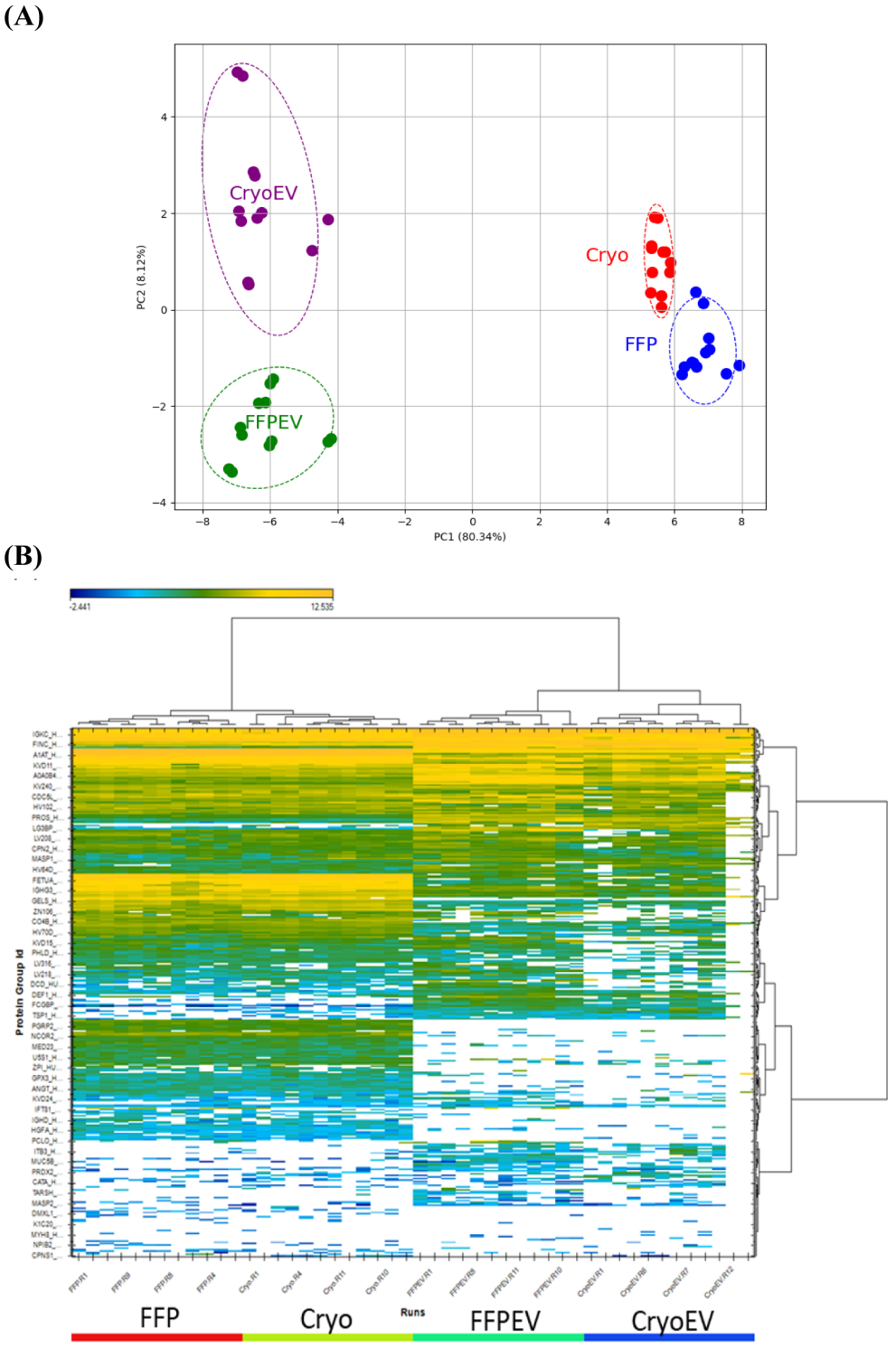

Figure 5. PCA and hierarchical clustering heatmap of the across the four samples. (A) Principal component analysis (PCA) of four sample groups, with axes representing loadings on components 1 and 2. (B) The blue color signifies low, and yellow color indicates high expression levels of the proteins identified in FFP, Cryo, FFPEV, and CryoEV. PC1: principal component 1; PC2: principal component 2; FFP: fresh frozen plasma; Cryo: cryoprecipitate; FFPEV: extracellular vesicles derived from fresh frozen plasma; CryoEV: extracellular vesicles were derived from cryoprecipitate.

identified in this study. One protein, alpha-2-macroglobulin, was common to both groups (Figure 4B).

To visualize and compare the different sample types, based on their protein expression, a principal component analysis (PCA) was performed. The results, as shown in Figure 5A, further highlighted the differences in protein expression among the different sample groups. The analysis revealed that EVs from both cryoprecipitate and FFP exhibited distinct protein expression patterns compared to those of their originating fluids. While the two original sample groups (FFP and cryoprecipitate) display very similar protein expression patterns, EVs derived from both cryoprecipitate and FFP displayed distinct protein expression profiles, as evidenced by their separation in PCA. This separation is driven by principal

https://doi.org/10.1021/acs.jproteome.4c00417
J. Proteome Res. 2024, 23, 4508−4522

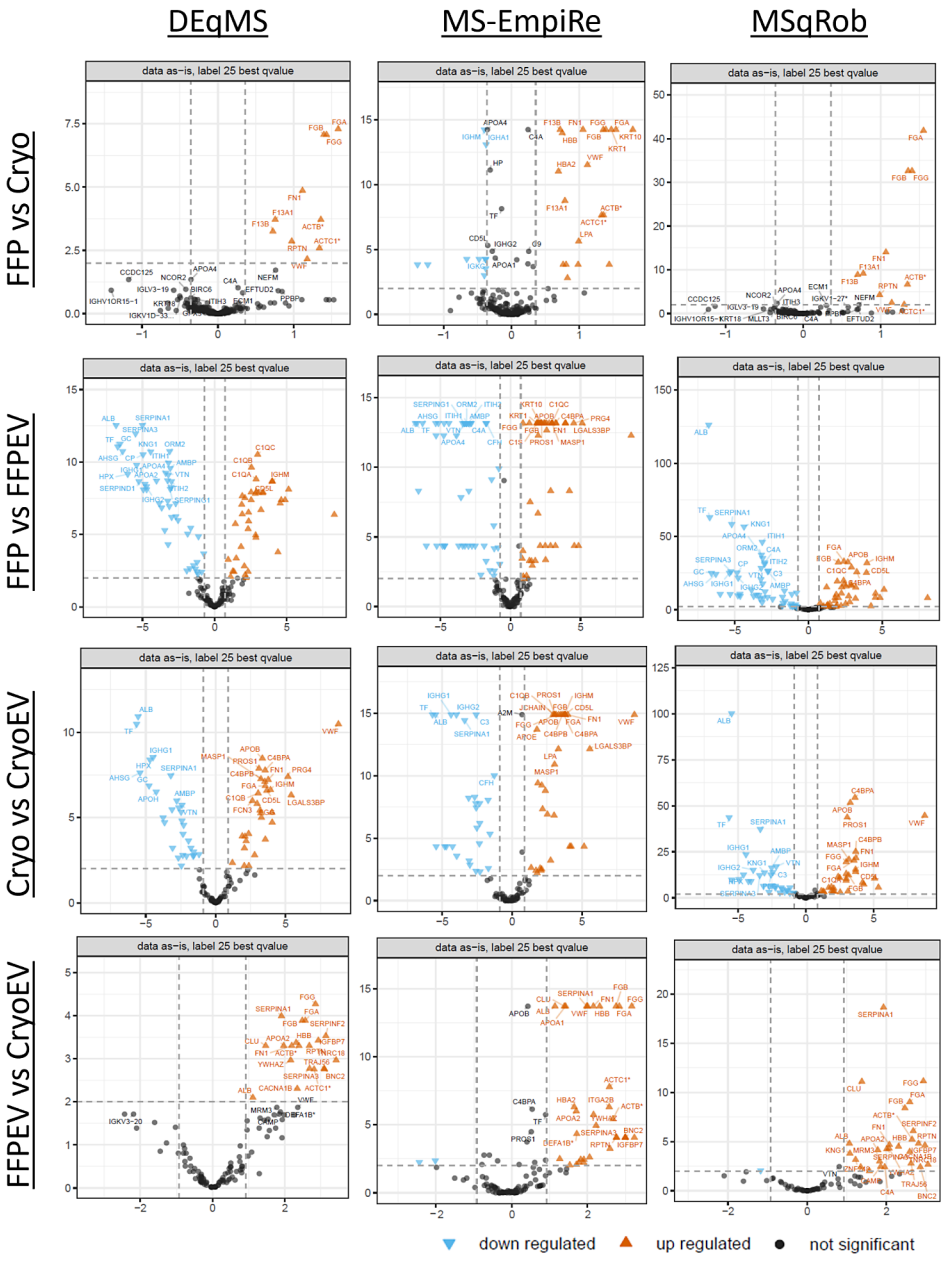

Figure 6. The differential expressed proteins across four sample groups, visualized by volcano plots produced using MS-DAP R package. Proteins found in different sample types (FFP, Cryo, FFPEV, CryoEV) were compared using three different algorithms using the R package MS-DAP: (1) DEqMS, (2) Ms-EmpiRe, and (3) MSqRob. FFP: fresh frozen plasma; Cryo: cryoprecipitate; FFPEV: extracellular vesicles derived from fresh frozen plasma; CryoEV: extracellular vesicles derived from cryoprecipitate.

component 1 (PC1, 80.34%). This result demonstrates the unique protein patterns of EVs compared to their originating fluids.

Given that we observed global differences among the samples, we further investigated the differential protein expression patterns in all samples in more detail. Based on the protein expression profiling, a heatmap was generated through two-dimensional hierarchical clustering of distinct clusters (Figure 5B). As indicated by the top dendrograms, it is divided into two main groups, with the first group consisting of the neat samples and the EVs in the second group. In addition, the right dendrograms showed that clusters consisted of a high protein cluster, represented in yellow, and a low protein cluster, shown in blue, across the four sample groups. As two distinct sample groups, the originated fluids, FFP and cryoprecipitate, exhibited different protein profiles that can be observed.

Differential Protein Expression Analysis Using MS-DAP

Raw MS data were analyzed using Spectronaut and subsequently imported into the MS-DAP downstream pipeline. Three different statistical methods DEqMS, MS-EmpiRe, and MsqRob were employed to analyze differential protein expression across the four sample groups in a pairwise manner. The result for each comparison by each method was visualized in a volcano plot where the top 25 proteins with the best q value were labeled (Figure 6).

In the first sample group comparison (FFP vs cryoprecipitate), we can apply some prior knowledge about the composition of cryoprecipitate to interpret what was observed.

https://doi.org/10.1021/acs.jproteome.4c00417
J. Proteome Res. 2024, 23, 4508−4522

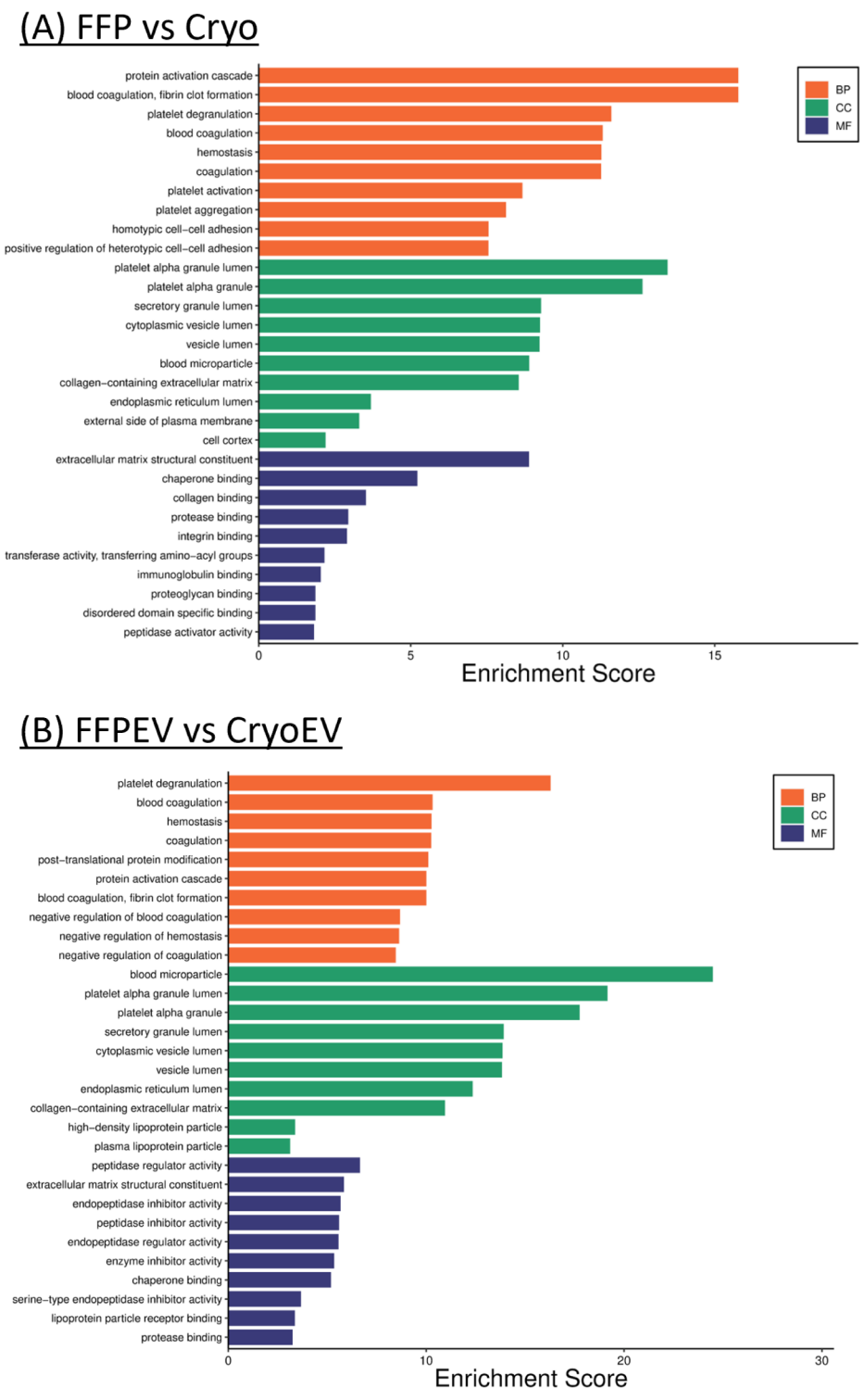

Figure 7. Enriched gene ontology (GO) terms for the differentially expressed proteins (DEPs) in FFP vs cryoprecipitate (Cryo) and FFPEV vs CryoEV. The identified DEPs were subjected to GO enrichment analysis: (A) FFP vs Cryo and (B) FFP vs EVs derived from Cryo (CryoEV). The GO terms were categorized into biological processes (BP), cellular components (CC), and molecular functions (MF). The top 10 pathways for each category are displayed.

Cryoprecipitate, as a clinical product, is highly enriched for certain key proteins including fibrinogen, factor VIII, von Willebrand factor, factor XIII, and fibronectin. Using a stringent method that classifies a protein as differentially expressed (DEP) only if it meets criteria in two out of three statistical methods, a total of 10 DEPs were identified (Supplementary Table S6). As expected, this method successfully identified all of the aforementioned proteins, which are highly enriched in cryoprecipitate, as DEPs. In addition, it also identified different forms of actin and repetin (RPTN) as DEPs. Notably, only the Ms-EmpiRe algorithm indicated decreased levels of certain proteins such as immunoglobulin heavy constant mu (IGHM),

https://doi.org/10.1021/acs.jproteome.4c00417
J. Proteome Res. 2024, 23, 4508−4522

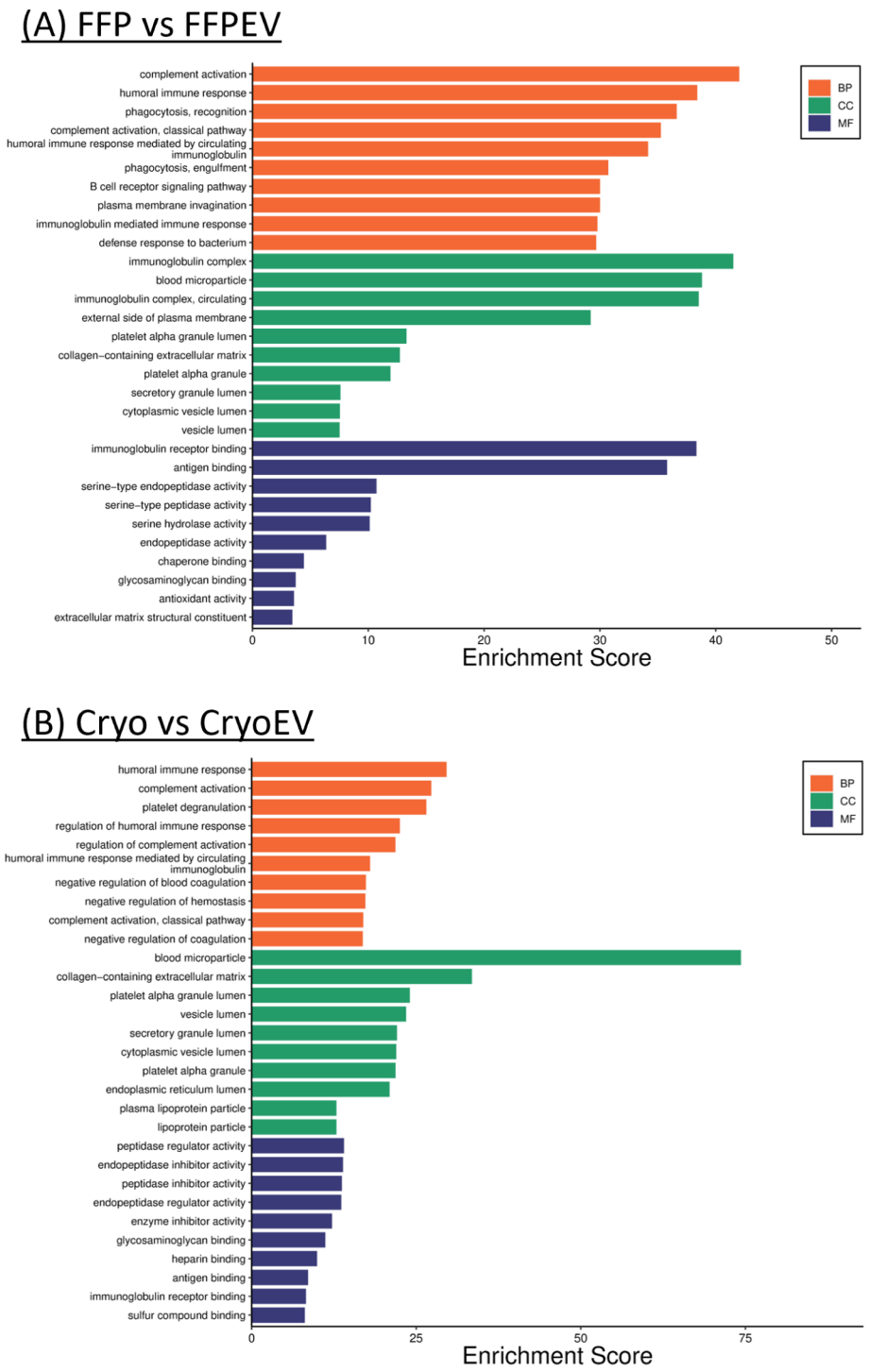

Figure 8. Enriched gene ontology (GO) terms for the differentially expressed proteins (DEPs) in FFP vs FFPEV and Cryo vs CryoEV. The identified DEPs were subjected to GO enrichment analysis: (A) FFP vs FFPEV and (B) Cryo vs EVs derived from Cryo (CryoEV). The GO terms were categorized into biological processes (BP), cellular components (CC), and molecular functions (MF). The top 10 pathways for each category are displayed.

immunoglobulin heavy constant alpha 1 (IGHA1), and immunoglobulin kappa constant (IGKC) in cryoprecipitate.

In the second sample group, comparing FFP versus EVs derived from FFP, a total of 87 DEPs were identified (Supplementary Table S7). Complement C1qC chain (C1QC) was found to increase in EVs from FFP across all algorithms. Both the Ms-Empire and MsqRob algorithms identified additional upregulated proteins, including apolipoprotein B protein (APOB) and FGB. Consistently across the three algorithms, several proteins showed decreased levels in EVs from FFP compared to FFP, including ALB, alpha 2-HS glycoprotein (AHSG), interalpha trypsin inhibitor, heavy chain 1 (ITIH1), interalpha trypsin inhibitor, heavy chain 2 (ITIH2), and vitronectin (VTN).

Between cryoprecipitate and its derived EVs, a similar trend was observed in the upregulation of proteins in EVs from

https://doi.org/10.1021/acs.jproteome.4c00417
J. Proteome Res. 2024, 23, 4508−4522

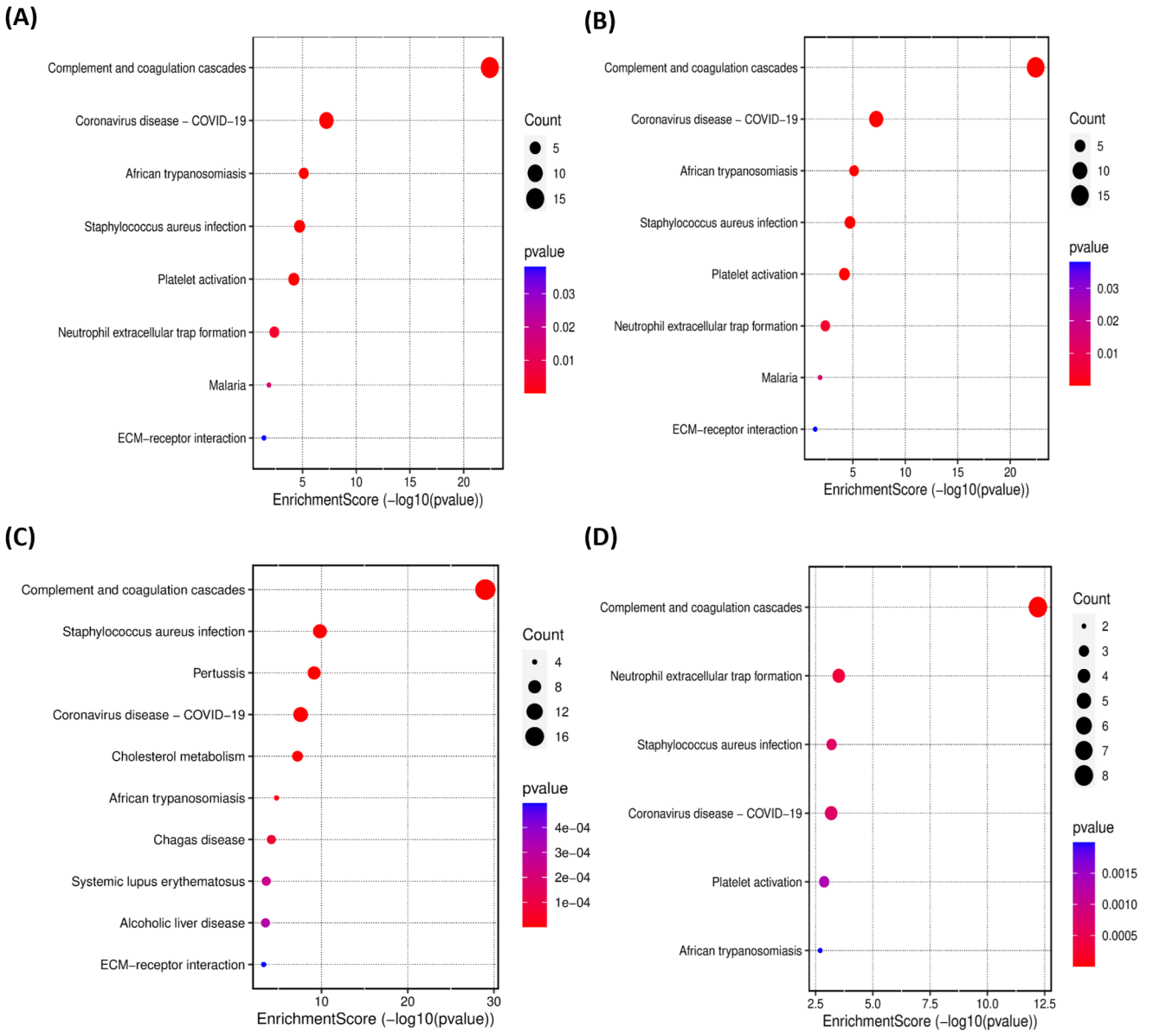

Figure 9. KEGG (Kyoto Encyclopedia of Genes and Genomes) pathway analysis for the DEPs. These figures illustrated the results of GO enrichment analysis comparing four pairs of sample groups: (A) FFP vs Cryo, (B) FFP vs FFPEV, (C) Cryo vs CryoEV, and (D) FFPEV vs CryoEV.

cryoprecipitate, including VWF, FGA, FGG, and FN1, and an elevated level of APOB. Mirroring the trend seen in EVs from FFP, EVs from cryoprecipitate also exhibited downregulated levels of TF, ALB, and serpin family A member 1 (SERPINA1). Overall, a total of 61 DEPs were identified (Supplementary Table S8).

The last sample group compared EVs from FFP with EVs from cryoprecipitate, the fewest DEP at 25, and only revealed elevated proteins across all three algorithms (Supplementary Table S9). The proteins, including FGG, FGA, FGB, SERPINA1, serpin family A member 3 (SERPINA3), FN1, ALB, clusterin (CLU), basonuclin zinc finger protein 2 (BNC2), and insulin-like growth factor binding protein 7 (IGFBP7), were all increased in EVs derived from cryoprecipitate compared to EVs from FFP.

The GO Enrichment and KEGG Analysis of Differentially Expressed Proteins in FFP, Cryoprecipitate, and Their Derived EVs

To determine what pathways and potential functional roles the DEPs have, gene ontology (GO) term and enrichment analyses were conducted to elucidate the functions and biological processes associated with differentially expressed proteins (DEPs) across four sample groups. The analysis of GO terms for biological processes revealed that these DEPs were involved in key areas: response to a cellular component (CC), biological processes (BP), and molecular functions (MF).

In comparison between FFP and cryoprecipitate, the GO terms for BP indicated that all DEPs were involved in several key processes: protein activation cascade, blood coagulation, fibrin clot formation, and platelet degranulation (Figure 7A). Regarding the GO terms for CC, there was an enrichment in the platelet alpha granule lumen and platelet alpha granule domains in cryoprecipitate. Furthermore, the MF GO terms

https://doi.org/10.1021/acs.jproteome.4c00417
J. Proteome Res. 2024, 23, 4508–4522

were particularly enriched in extracellular matrix structural constituent and chaperone binding, again more significantly in cryoprecipitate.

A comparison of the DEPs was subsequently made between the EVs derived from FFP and cryoprecipitate. The GO terms of BP were enriched in platelet degranulation and blood coagulation in EVs from cryoprecipitate as shown in Figure 7B. The GO terms of CC indicated significant enrichment in blood microparticles, with the second highest enrichment observed in the platelet alpha granule lumen. Moreover, the GO terms for MF indicated enrichment in peptidase regulator activity and extracellular matrix structural constituents.

In the next sample group, FFP compared to EVs derived from FFP (FFPEV), the GO terms for BP were enriched in complement activation and humoral immune response in FFPEV (Figure 8A). The GO terms for CC indicated enrichment in the immunoglobin complex and blood microparticle. The GO terms for MF displayed enrichment for immunoglobulin receptor binding and antigen binding.

In the final comparison between cryoprecipitate and EVs derived from cryoprecipitate (CryoEV), the GO term of BP was enriched in humoral immune response and complement activation in CryoEV (Figure 8B). Notably, the GO term of CC showed a high enrichment score for blood microparticle, followed by collagen-containing extracellular matrix in CryoEV. Furthermore, the GO terms of MF were enriched in peptidase regulator activity, endopeptidase inhibitor activity, and peptidase inhibitor activity in CryoEV compared to cryoprecipitate.

To investigate the potential functions and signaling pathways involved for DEPs, the KEGG (Kyoto Encyclopedia of Genes and Genomes) database was interrogated (Figure 9). The sample group comparison between FFP and cryoprecipitate revealed that most DEPs were enriched in complement and coagulation cascades, and coronavirus disease (COVID 19) pathways in cryoprecipitate, compared to FFP. Interestingly, this trend continued to show similar results in the other two sample group comparisons: FFP vs FFPEV, and cryoprecipitate vs CryoEV. In the comparison between FFPEV and CryoEV, most DEPs were also enriched in complement and coagulation cascades; however, the second highest enrichment was observed in neutrophil extracellular trap formation, specifically in CryoEV.

DISCUSSION

FFP and cryoprecipitate are clinically significant blood components used in transfusions. Both fluids contain EVs, which can be enriched from the originating fluid and subsequently validated for successful isolation. Given the capacity of EVs to carry various bioactive molecules, including proteins, it is essential to determine their protein profiles. However, an in-depth proteomic profile of EVs derived from both fluids, particularly from cryoprecipitate (CryoEV), has not yet been extensively studied. To the best of our knowledge, this is the first study to not only isolate and obtain a protein profile of EVs from cryoprecipitate but also to do so in accordance with international guidelines.[22] Using semiquantitative DIA mass spectrometry, and with a relatively short runtime of 30 min, we have successfully profiled and compared the proteins in FFP, cryoprecipitate, FFPEV, and CryoEV. We found that the originating fluids (FFP and cryoprecipitate) have similar protein profiles, as do their respective EVs (FFPEV and CryoEV). However, these profiles are distinct from each other. When comparing the proteins identified to the top 100 proteins found in EVs listed in Vesiclepedia, only a minor proportion overlapped. This can be explained by the variations in the source and isolation methods of the EVs. Therefore, the top 100 proteins cannot be strictly termed as EV-specific markers or enriched proteins, a limitation previously acknowledged.[39]

We presently employed a mass spectrometry downstream analysis pipeline (MS-DAP) to identify DEPs after processing the MS output. While various statistical models exist for quantifying and detecting DEPs, we utilized MS-DAP, which aimed to improve detection using multiple statistical models.[27] Our approach was aimed at achieving a more accurate and consistent identification of DEPs. The DEqMS model enhances the typical approach of moderated *t*-statistics used in protein abundance analysis by integrating the count of quantified peptides per protein.[28] In contrast, the MS-EmpiRe and MSqRob models work directly with peptide abundance values for estimating DEPs, bypassing the need for peptide-to-protein rollup.[29,40] To increase the stringency in DEP identification, we selected proteins that were identified in two of the three models. To give confidence in this approach, we were successful in identifying proteins that have previously been identified as enriched and are clinically important and active in cryoprecipitate. These proteins include fibrinogen, factor VIII, von Willebrand factor, factor XIII, and fibronectin.[41]

In our study, we observed that the expression of tissue factor (F3), a critical initiator of blood coagulation, was not detectable in the neat blood components or in their derived extracellular vesicles (EVs). This could be explained by the levels of tissue factor in the isolated EV population being below the limit of detection, which potentially could be detected using a potentially more sensitive activity assay.[42] Another significant finding was the elevated levels of APOB, the main protein in low-density lipoproteins (LDL), in both EV samples. Generally, isolating EVs from plasma presents challenges due to the low concentration of EVs compared to lipoproteins, as well as the overlap in size and density between EVs and lipoproteins.[43] However, a recent study has shown that the so-called "contamination" of EV preparations with plasma proteins may actually be due to the natural formation of a protein corona around EVs in blood plasma.[44] Proteins such as ApoA1, ApoB, ApoC3, ApoE, complement factor 3 and 4B, fibrinogen α-chain, and immunoglobulin heavy constant γ2 and γ4 chains were identified as part of the corona forming around EVs in plasma, some of which were also detected in this study from the isolated EVs. In addition, large protein complexes can also associate with EVs' surface. The recently released MISEV 2023 guidelines have classified these proteins in category 5, blood-derived corona proteins.[22] The protein corona of the EVs was found to be functional and plays an important role in the EVs' ability to induce their functional effects.[44,45] It is therefore possible that the proteins identified as DEPs in CryoEV compared to FFPEV may be due to the environment of cryoprecipitate from which the EVs were derived. Potentially, proteins such as fibrinogen and fibronectin are more enriched because they can form a corona or a complex around CryoEV. This field of research is relatively new, and the mechanism of corona formation is still under investigation, which can have an impact on understanding the bioactivity and biodistribution of EVs.[46]

The human plasma proteome is extremely complex, spanning approximately 10 orders of magnitude in concentrations. Highly abundant proteins such as albumin are in the mg/mL range, while some cytokines are in the pg/mL range.[47] Given such a

https://doi.org/10.1021/acs.jproteome.4c00417
J. Proteome Res. 2024, 23, 4508−4522

large dynamic range, it represents a major challenge for the quantitative analysis of neat plasma, including samples derived from it such as cryoprecipitate and EVs. In this study, we have profiled around 360 proteins across all the sample groups, spanning 4 magnitudes of concentrations, which is consistent with the 4−6 log of dynamic range for mass spectrometers.[48] A recent study comparing different EV isolation methods from plasma showed that EVs isolated via SEC were suitable for clinically relevant samples and resulted in the identification of 281 proteins by mass spectrometry, which was comparable to this study.[49] The number of proteins identified can be improved via several strategies that can be employed to gain additional depth. Techniques such as sample fractionation, depletion, and improvement in mass spectrometers can mitigate some of the challenges posed by the proteome.[50] In addition, since lipids are a major component of EVs, lipidomics should be conducted to gain additional information about the molecular composition of those EVs found in FFP and cryoprecipitate.

In conclusion, this work has provided novel insights into the proteomic landscape of cryoprecipitate, FFP, and their derived EVs. For the first time, we have profiled proteins associated with CryoEV and found that they resemble those found in FFPEV, more than those found in their originating fluid. Moreover, this work represents an important step forward in the profiling of EVs derived from clinically important blood components, such as cryoprecipitate.

■ ASSOCIATED CONTENT

Supporting Information

The Supporting Information is available free of charge at https://pubs.acs.org/doi/10.1021/acs.jproteome.4c00417.

Liquid chromatography (LC) conditions (Supplementary Table S1); SWATH variable windows (Supplementary Table S2); protein abundance rank and their classification (Supplementary Table S3); KEGG coagulation and complement (Supplementary Table S4); top 100 proteins previously identified in EVs (sourced from Vesiclepedia; Supplementary Table S5); list of DEP for FFP vs cryoprecipitate discovered using multiple algorithms (Supplementary Table S6); list of DEP for FFP vs FFPEV discovered using multiple algorithms (Supplementary Table S7); list of DEP for Cryo vs CryoEV discovered using multiple algorithms (Supplementary Table S8); list of DEP for FFPEV vs CryoEV discovered using multiple algorithms (Supplementary Table S9); data analysis parameters for Spectronaut (Supplementary Figure S1); export schema from Spectronaut for downstream processing by MS-DAP (Supplementary Figure S2); MS-DAP settings (Supplementary Figure S3); FFP and cryoprecipitate-EV Western blots (Supplementary Figure S4); number of detected peptides (left) and proteins (right) (Supplementary Figure S5) (PDF)

■ AUTHOR INFORMATION

Corresponding Author

Ji Hui Hwang − *School of Biomedical Sciences, Faculty of Health, Queensland University of Technology, Brisbane, Qld 4000, Australia; Research and Development, Australian Red Cross Lifeblood, Brisbane, QLD 4059, Australia;* orcid.org/0009-0005-1912-4921; Email: jihui.hwang@qut.edu.au

Authors

Andrew Lai − *UQ Centre for Clinical Research, Faculty of Medicine, University of Queensland, Brisbane, QLD 4006, Australia*

John-Paul Tung − *School of Biomedical Sciences, Faculty of Health, Queensland University of Technology, Brisbane, Qld 4000, Australia; Research and Development, Australian Red Cross Lifeblood, Brisbane, QLD 4059, Australia; Faculty of Medicine, University of Queensland, Brisbane, QLD 4006, Australia; School of Health, University of the Sunshine Coast, Sippy Downs, QLD 4556, Australia*

Damien G Harkin − *School of Biomedical Sciences, Faculty of Health, Queensland University of Technology, Brisbane, Qld 4000, Australia; Research and Development, Australian Red Cross Lifeblood, Brisbane, QLD 4059, Australia*

Robert L Flower − *School of Biomedical Sciences, Faculty of Health, Queensland University of Technology, Brisbane, Qld 4000, Australia; Research and Development, Australian Red Cross Lifeblood, Brisbane, QLD 4059, Australia*

Natalie M Pecheniuk − *School of Biomedical Sciences, Faculty of Health, Queensland University of Technology, Brisbane, Qld 4000, Australia; Research and Development, Australian Red Cross Lifeblood, Brisbane, QLD 4059, Australia*

Complete contact information is available at: https://pubs.acs.org/10.1021/acs.jproteome.4c00417

Notes

The authors declare no competing financial interest.

■ ACKNOWLEDGMENTS

This work was supported by a Queensland University of Technology Women in Research Grant (NMP). JHH is the holder of an Australian Government Research Training Program (RTP) Scholarship. Australian Governments fund Australian Red Cross Lifeblood for the provision of blood, blood components, and services to the Australian Community. The authors acknowledge the facilities and the scientific and technical assistance of the Microscopy Australia Research Facility at the Centre for Microscopy and Microanalysis, The University of Queensland.

■ REFERENCES

(1) Muraoka, S.; Jedrychowski, M. P.; Yanamandra, K.; Ikezu, S.; Gygi, S. P.; Ikezu, T. Proteomic Profiling of Extracellular Vesicles Derived from Cerebrospinal Fluid of Alzheimer's Disease Patients: A Pilot Study. *Cells* **2020**, *9* (9), 1959.

(2) Kowal, J.; Arras, G.; Colombo, M.; Jouve, M.; Morath, J. P.; Primdal-Bengtson, B.; Dingli, F.; Loew, D.; Tkach, M.; Théry, C. Proteomic comparison defines novel markers to characterize heterogeneous populations of extracellular vesicle subtypes. *Proc. Natl. Acad. Sci. U. S. A.* **2016**, *113* (8), No. E968−977.

(3) Muraoka, S.; Hirano, M.; Isoyama, J.; Ishida, M.; Tomonaga, T.; Adachi, J. Automated Proteomics Sample Preparation of Phosphatidylserine-Positive Extracellular Vesicles from Human Body Fluids. *ACS Omega* **2022**, *7* (45), 41472−41479.

(4) Hoshino, A.; Kim, H. S.; Bojmar, L.; Gyan, K. E.; Cioffi, M.; Hernandez, J.; Zambirinis, C. P.; Rodrigues, G.; Molina, H.; Heissel, S.; et al. Extracellular Vesicle and Particle Biomarkers Define Multiple Human Cancers. *Cell* **2020**, *182* (4), 1044−1061.e1018.

(5) Regev-Rudzki, N.; Wilson, D. W.; Carvalho, T. G.; Sisquella, X.; Coleman, B. M.; Rug, M.; Bursac, D.; Angrisano, F.; Gee, M.; Hill, A. F.; et al. Cell-cell communication between malaria-infected red blood cells via exosome-like vesicles. *Cell* **2013**, *153* (5), 1120−1133.

(6) Xu, R.; Rai, A.; Chen, M.; Suwakulsiri, W.; Greening, D. W.; Simpson, R. J. Extracellular vesicles in cancer—implications for future improvements in cancer care. *Nat. Rev. Clin. Oncol.* **2018**, *15* (10), 617−638.
(7) Mitchell, M. D.; Peiris, H. N.; Kobayashi, M.; Koh, Y. Q.; Duncombe, G.; Illanes, S. E.; Rice, G. E.; Salomon, C. Placental exosomes in normal and complicated pregnancy. *Am. J. Obstet Gynecol.* **2015**, *213* (4 Suppl), S173−S181.
(8) Ailawadi, S.; Wang, X.; Gu, H.; Fan, G. C. Pathologic function and therapeutic potential of exosomes in cardiovascular disease. *Biochim. Biophys. Acta* **2015**, *1852* (1), 1−11.
(9) Pocsfalvi, G.; Stanly, C.; Vilasi, A.; Fiume, I.; Capasso, G.; Turiák, L.; Buzas, E. I.; Vékey, K. Mass spectrometry of extracellular vesicles. *Mass Spectrom. Rev.* **2016**, *35* (1), 3−21.
(10) Couch, Y.; Buzàs, E. I.; Di Vizio, D.; Gho, Y. S.; Harrison, P.; Hill, A. F.; Lötvall, J.; Raposo, G.; Stahl, P. D.; Théry, C.; et al. A brief history of nearly EV-erything - The rise and rise of extracellular vesicles. *J. Extracell. Vesicles* **2021**, *10* (14), No. e12144.
(11) Palviainen, M.; Saraswat, M.; Varga, Z.; Kitka, D.; Neuvonen, M.; Puhka, M.; Joenväärä, S.; Renkonen, R.; Nieuwland, R.; Takatalo, M.; et al. Extracellular vesicles from human plasma and serum are carriers of extravesicular cargo-Implications for biomarker discovery. *PLoS One* **2020**, *15* (8), No. e0236439.
(12) Mallia, A.; Gianazza, E.; Zoanni, B.; Brioschi, M.; Barbieri, S. S.; Banfi, C. Proteomics of Extracellular Vesicles: Update on Their Composition, Biological Roles and Potential Use as Diagnostic Tools in Atherosclerotic Cardiovascular Diseases. *Diagnostics (Basel)* **2020**, *10*, 843.
(13) Tu, C.; Rudnick, P. A.; Martinez, M. Y.; Cheek, K. L.; Stein, S. E.; Slebos, R. J.; Liebler, D. C. Depletion of abundant plasma proteins and limitations of plasma proteomics. *J. Proteome Res.* **2010**, *9* (10), 4982−4991.
(14) Keshishian, H.; Burgess, M. W.; Specht, H.; Wallace, L.; Clauser, K. R.; Gillette, M. A.; Carr, S. A. Quantitative, multiplexed workflow for deep analysis of human blood plasma and biomarker discovery by mass spectrometry. *Nat. Protoc.* **2017**, *12* (8), 1683−1701.
(15) Puhm, F.; Boilard, E.; Machlus, K. R. Computationally Driven Discovery in Coagulation. *Arterioscler., Thromb., Vasc. Biol.* **2021**, *41* (1), 87−96.
(16) Ma, S. R.; Xia, H. F.; Gong, P.; Yu, Z. L. Red Blood Cell-Derived Extracellular Vesicles: An Overview of Current Research Progress, Challenges, and Opportunities. *Biomedicines* **2023**, *11* (10), 2798.
(17) Cho, K. C.; Clark, D. J.; Schnaubelt, M.; Teo, G. C.; Leprevost, F. D. V.; Bocik, W.; Boja, E. S.; Hiltke, T.; Nesvizhskii, A. I.; Zhang, H. Deep Proteomics Using Two Dimensional Data Independent Acquisition Mass Spectrometry. *Anal. Chem.* **2020**, *92* (6), 4217−4225.
(18) Gillet, L. C.; Navarro, P.; Tate, S.; Röst, H.; Selevsek, N.; Reiter, L.; Bonner, R.; Aebersold, R. Targeted data extraction of the MS/MS spectra generated by data-independent acquisition: a new concept for consistent and accurate proteome analysis. *Mol. Cell. Proteomics* **2012**, *11* (6), 1400−1410.
(19) Li, Q. K.; Chen, J.; Hu, Y.; Höti, N.; Lih, T.-S. M.; Thomas, S. N.; Chen, L.; Roy, S.; Meeker, A.; Shah, P.; et al. Proteomic characterization of primary and metastatic prostate cancer reveals reduced proteinase activity in aggressive tumors. *Sci. Rep.* **2021**, *11* (1), 18936.
(20) Ludwig, C.; Gillet, L.; Rosenberger, G.; Amon, S.; Collins, B. C.; Aebersold, R. Data-independent acquisition-based SWATH-MS for quantitative proteomics: a tutorial. *Mol. Syst. Biol.* **2018**, *14* (8), No. e8126.
(21) Collins, B. C.; Hunter, C. L.; Liu, Y.; Schilling, B.; Rosenberger, G.; Bader, S. L.; Chan, D. W.; Gibson, B. W.; Gingras, A.-C.; Held, J. M.; et al. Multi-laboratory assessment of reproducibility, qualitative and quantitative performance of SWATH-mass spectrometry. *Nat. Commun.* **2017**, *8* (1), 291.
(22) Welsh, J. A.; Goberdhan, D. C. I.; O'Driscoll, L.; Buzas, E. I.; Blenkiron, C.; Bussolati, B.; Cai, H.; Di Vizio, D.; Driedonks, T. A. P.; Erdbrügger, U.; et al. Minimal information for studies of extracellular vesicles (MISEV2023): From basic to advanced approaches. *J. Extracell. Vesicles* **2024**, *13* (2), No. e12404.
(23) Mastronarde, D. N. Automated electron microscope tomography using robust prediction of specimen movements. *J. Struct. Biol* **2005**, *152* (1), 36−51.
(24) Bruderer, R.; Bernhardt, O. M.; Gandhi, T.; Miladinović, S. M.; Cheng, L.-Y.; Messner, S.; Ehrenberger, T.; Zanotelli, V.; Butscheid, Y.; Escher, C.; et al. Extending the limits of quantitative proteome profiling with data-independent acquisition and application to acetaminophen-treated three-dimensional liver microtissues*[S]. *Mol. Cell. Proteomics* **2015**, *14* (5), 1400−1410.
(25) *R: A language and environment for statistical computing*; R Foundation for Statistical Computing, 2023. https://www.R-project.org/.
(26) *RStudio: Integrated Development Environment for R*; Posit Software: PBC, Boston, MA, USA, 2023. http://www.posit.co/.
(27) Koopmans, F.; Li, K. W.; Klaassen, R. V.; Smit, A. B. MS-DAP Platform for Downstream Data Analysis of Label-Free Proteomics Uncovers Optimal Workflows in Benchmark Data Sets and Increased Sensitivity in Analysis of Alzheimer's Biomarker Data. *J. Proteome Res.* **2023**, *22* (2), 374−386.
(28) Zhu, Y.; Orre, L. M.; Zhou Tran, Y.; Mermelekas, G.; Johansson, H. J.; Malyutina, A.; Anders, S.; Lehtiö, J. DEqMS: A Method for Accurate Variance Estimation in Differential Protein Expression Analysis. *Mol. Cell. Proteomics* **2020**, *19* (6), 1047−1057.
(29) Ammar, C.; Gruber, M.; Csaba, G.; Zimmer, R. MS-EmpiRe Utilizes Peptide-level Noise Distributions for Ultra-sensitive Detection of Differentially Expressed Proteins. *Mol. Cell. Proteomics* **2019**, *18* (9), 1880−1892.
(30) Goeminne, L. E.; Gevaert, K.; Clement, L. Peptide-level robust ridge regression improves estimation, sensitivity, and specificity in data-dependent quantitative label-free shotgun proteomics. *Mol. Cell. Proteomics* **2016**, *15* (2), 657−668.
(31) *PyCharm software (version 2023.3)*; published by JetBrains and available from https://www.jetbrains.com/pycharm/. 2003.
(32) Hunter, J. D. Matplotlib: a 2D Graphics Environment. *Comput. Sci. Eng.* **2007**, *9* (3), 90−95.
(33) Waskom, M. L. Seaborn: statistical data visualization. *J. Open Source Software* **2021**, *6* (60), 3021.
(34) Chitti, S. V.; Gummadi, S.; Kang, T.; Shahi, S.; Marzan, A. L.; Nedeva, C.; Sanwlani, R.; Bramich, K.; Stewart, S.; Petrovska, M.; et al. Vesiclepedia 2024: an extracellular vesicles and extracellular particles repository. *Nucleic Acids Res.* **2023**, *52*, D1694−D1698.
(35) Kanehisa, M.; Furumichi, M.; Sato, Y.; Kawashima, M.; Ishiguro-Watanabe, M. KEGG for taxonomy-based analysis of pathways and genomes. *Nucleic Acids Res.* **2023**, *51* (D1), D587−D592.
(36) Yu, G.; Wang, L.-G.; Han, Y.; He, Q.-Y. clusterProfiler: an R package for comparing biological themes among gene clusters. *Omics: A J. Integrat. Biol.* **2012**, *16* (5), 284−287.
(37) Luo, W.; Brouwer, C. Pathview: an R/Bioconductor package for pathway-based data integration and visualization. *Bioinformatics* **2013**, *29* (14), 1830−1831.
(38) Tang, D.; Chen, M.; Huang, X.; Zhang, G.; Zeng, L.; Zhang, G.; Wu, S.; Wang, Y. SRplot: A free online platform for data visualization and graphing. *PLoS One* **2023**, *18* (11), No. e0294236.
(39) Chitti, S. V.; Gummadi, S.; Kang, T.; Shahi, S.; Marzan, A. L.; Nedeva, C.; Sanwlani, R.; Bramich, K.; Stewart, S.; Petrovska, M.; et al. Vesiclepedia 2024: an extracellular vesicles and extracellular particles repository. *Nucleic Acids Res.* **2024**, *52* (D1), D1694−d1698.
(40) Goeminne, L. J.; Gevaert, K.; Clement, L. Peptide-level Robust Ridge Regression Improves Estimation, Sensitivity, and Specificity in Data-dependent Quantitative Label-free Shotgun Proteomics. *Mol. Cell. Proteomics* **2016**, *15* (2), 657−668.
(41) Nair, P. M.; Rendo, M. J.; Reddoch-Cardenas, K. M.; Burris, J. K.; Meledeo, M. A.; Cap, A. P. Recent advances in use of fresh frozen plasma, cryoprecipitate, immunoglobulins, and clotting factors for transfusion support in patients with hematologic disease. *Semin Hematol.* **2020**, *57* (2), 73−82.
(42) Hisada, Y.; Mackman, N. Measurement of tissue factor activity in extracellular vesicles from human plasma samples. *Res. Pract Thromb Haemost.* **2019**, *3* (1), 44−48.

https://doi.org/10.1021/acs.jproteome.4c00417
J. Proteome Res. 2024, 23, 4508−4522

(43) Johnsen, K. B.; Gudbergsson, J. M.; Andresen, T. L.; Simonsen, J. B. What is the blood concentration of extracellular vesicles? Implications for the use of extracellular vesicles as blood-borne biomarkers of cancer. *Biochim. Biophys. Acta, Rev. Cancer* **2019**, *1871* (1), 109−116.
(44) Tóth, E. Á.; Turiák, L.; Visnovitz, T.; Cserép, C.; Mázló, A.; Sódar, B. W.; Försönits, A. I.; Petővári, G.; Sebestyén, A.; Komlósi, Z.; et al. Formation of a protein corona on the surface of extracellular vesicles in blood plasma. *J. Extracell. Vesicles* **2021**, *10* (11), No. e12140.
(45) Wolf, M.; Poupardin, R. W.; Ebner-Peking, P.; Andrade, A. C.; Blöchl, C.; Obermayer, A.; Gomes, F. G.; Vari, B.; Maeding, N.; Eminger, E.; et al. A functional corona around extracellular vesicles enhances angiogenesis, skin regeneration and immunomodulation. *J. Extracell. Vesicles* **2022**, *11* (4), No. e12207.
(46) Heidarzadeh, M.; Zarebkohan, A.; Rahbarghazi, R.; Sokullu, E. Protein corona and exosomes: new challenges and prospects. *Cell Commun. Signal.* **2023**, *21*, 1.
(47) Anderson, N. L.; Anderson, N. G. The Human Plasma Proteome: History, Character, and Diagnostic Prospects*. *Mol. Cell. Proteomics* **2002**, *1* (11), 845−867.
(48) Ren, A. H.; Diamandis, E. P.; Kulasingam, V. Uncovering the Depths of the Human Proteome: Antibody-based Technologies for Ultrasensitive Multiplexed Protein Detection and Quantification. *Mol. Cell. Proteomics* **2021**, *20*, 100155.
(49) Robinson, S. D.; Samuels, M.; Jones, W.; Stewart, N.; Eravci, M.; Mazarakis, N. K.; Gilbert, D.; Critchley, G.; Giamas, G. Confirming size-exclusion chromatography as a clinically relevant extracellular vesicles separation method from 1mL plasma through a comprehensive comparison of methods. *BMC Methods* **2024**, *1* (1), 7.
(50) MacCoss, M. J.; Alfaro, J. A.; Faivre, D. A.; Wu, C. C.; Wanunu, M.; Slavov, N. Sampling the proteome by emerging single-molecule and mass spectrometry methods. *Nat. Methods* **2023**, *20* (3), 339−346.

https://doi.org/10.1021/acs.jproteome.4c00417
J. Proteome Res. 2024, 23, 4508−4522